Supplemental Figures for Wang *et al*., 2019

Role of the chromosome architectural factor, SMCHD1, in X chromosome inactivation, gene regulation, and disease in humans

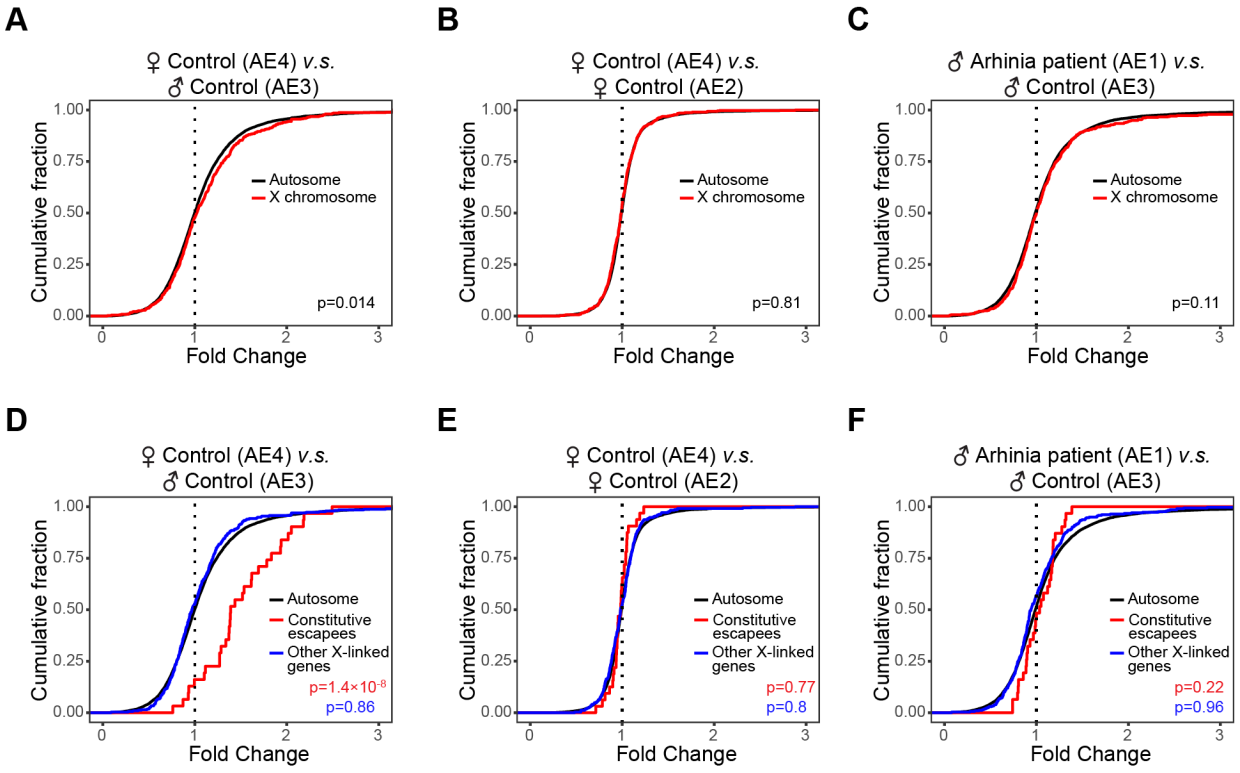

Figure S1. Upregulation of constitutive escapees in females relative to males.

(A) Cumulative distribution plots (CDPs) comparing fold changes for X-linked and autosomal genes between a female and a male control. *P*-values given by Wilcoxon ranked sum test (unpaired, one-sided).

(B) CDPs comparing fold changes for X-linked and autosomal genes between two female controls.

(C) CDPs comparing fold changes for X-linked and autosomal genes between two male controls.

(D) CDPs comparing fold changes for constitutive escapees (n=49), other X-linked genes (excluding facultative escapees and genes at the pseudo-autosomal regions), and autosomal genes between a female and a male control. *P*-values: constitutive escapees versus autosomal genes (black); other X-linked genes versus autosomal genes (blue).

(E) CDPs comparing fold changes for constitutive escapees, other X-linked genes, and autosomal genes between two female controls.

(F) CDPs comparing fold changes for constitutive escapees, other X-linked genes, and autosomal genes between two male controls.

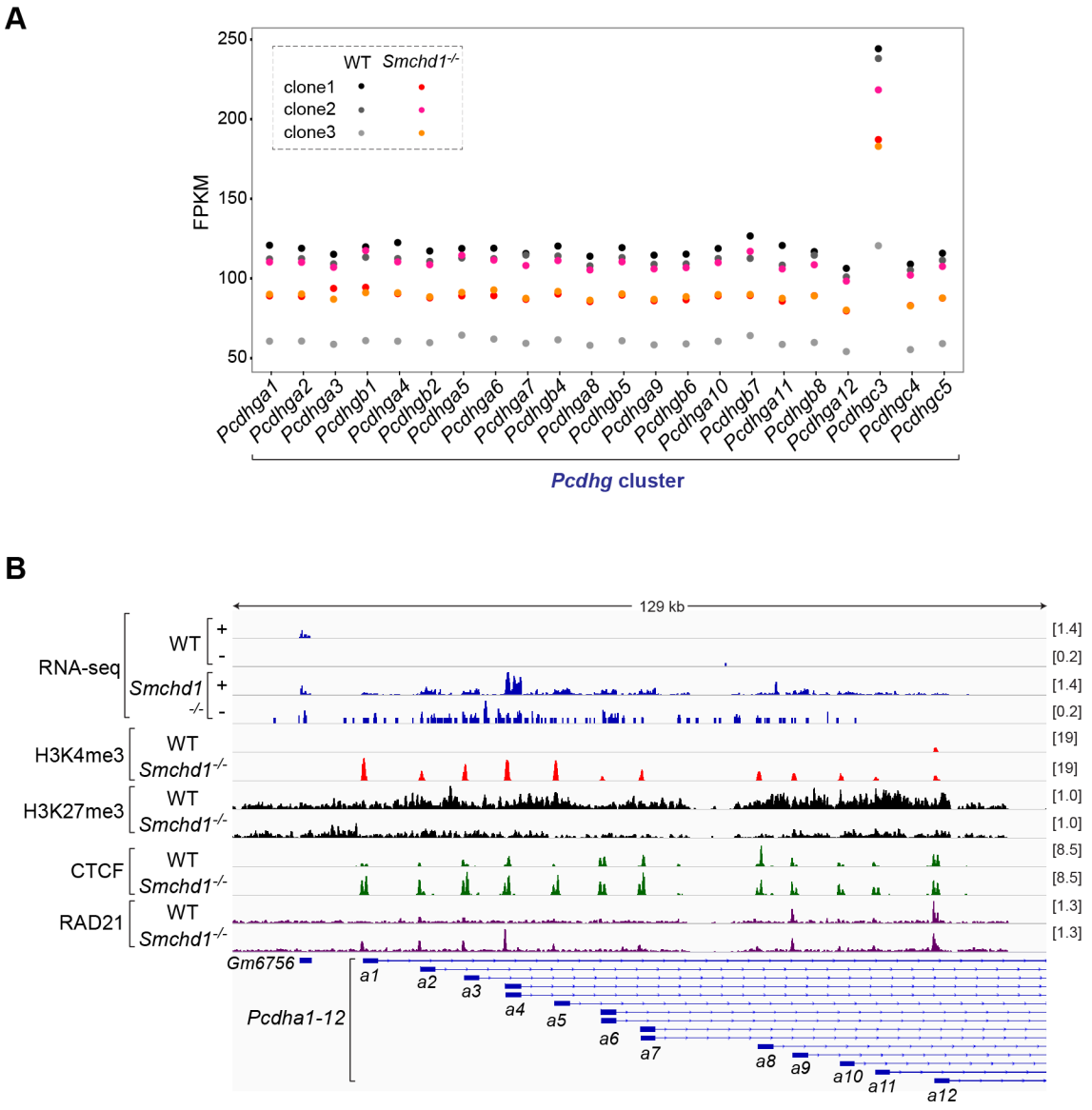

Figure S2. *Pcdhg* expression is not affected by *Smchd1* ablation in mouse NPCs.

(A) Dot plots showing the FPKMs of the 22 *Pcdhg* genes in WT (n=3) and *Smcdh1*$^{-/-}$ (n=3) mouse NPC clones.

(B) RNA-seq, H3K4me3, H3K27me3, CTCF, and RAD21 ChIP-seq (GSE99991) tracks at the *Pcdha1-12* region in WT (clone1) and *Smchd1*$^{-/-}$ (clone1) female mouse NPCs, with scales indicated in each track. Note that the scales for RNA-seq plus and minus strands were set differently to better visualize antisense transcription in *Smchd1*$^{-/-}$ cells. +, the plus strand. -, the minus strand. Also note that each of the *Pcdha1-12* alternate exons was marked by two adjacent CTCF ChIP-seq "peaks," as two CTCF-binding sites were present at each alternate exon (Guo et al., 2012; Monahan et al., 2012).

A

Patient ID	Mutation type	Nucleotide mutation	Exon	Amino acid alteration	Position	SMCHD1 abundance	SMCHD1 activity
AE1	Missense	g.2697032A>G	9	p.His348Arg	GHKL ATPase	No effect (Shaw *et al*, 2017)	Increased ATPase activity (Gurzau *et al*., 2018)
B1	Missense	g.2700840A>G	12	p.Asn524Ser	Extended region	No effect (Shaw *et al*, 2017)	Not tested
C1	Missense	g.2667029G>C	3	p.Leu141Phe	GHKL ATPase	No effect (Shaw *et al*, 2017)	Not tested
D1	Missense	g.2666992T>A	3	p.Met129Lys	GHKL ATPase	No effect (Shaw *et al*, 2017)	Not tested
E1	Missense	g.2667029G>C	3	p.Leu141Phe	GHKL ATPase	No effect (Shaw *et al*, 2017)	Not tested
W1	Missense	g.2700611G>C	11	p.Glu473Gln	Extended region	No effect (Shaw *et al*, 2017)	Not tested

B

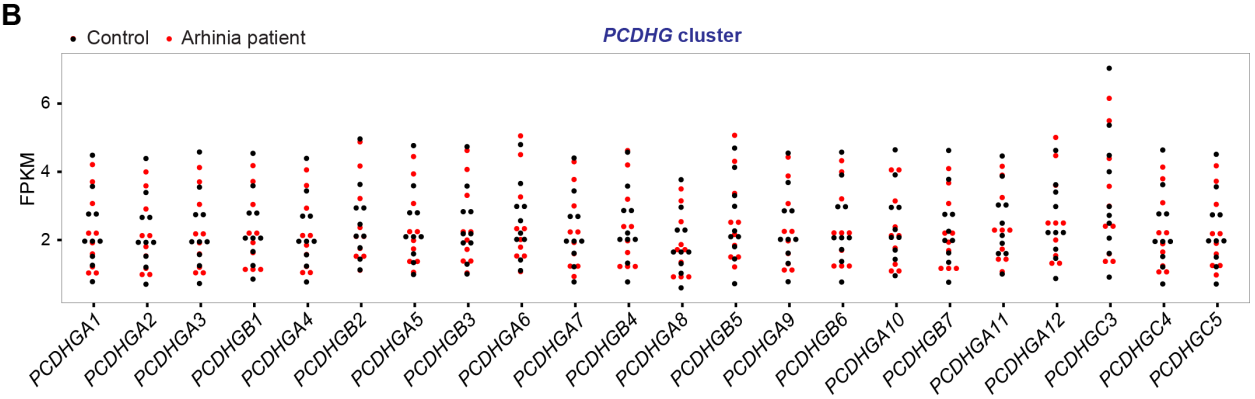

C

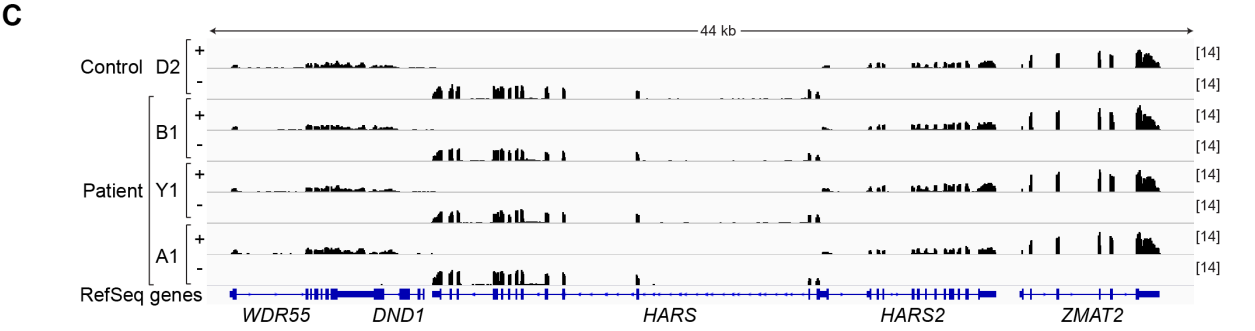

Figure S3. *PCDHB and PCDHG* expression in arhinia patients.

(A) A table listing the cohort of six male arhinia their associated *SMCHD1* mutations. Together with the four female arhinia patients included in Figure 1A, a total of 10 arhinia patients were included in our analysis of autosomal gene expression.

(B) Dot plots showing the FPKMs of the 22 *PCDHG* genes in LCLs of 10 arhinia patients (red) and 10 controls (black).

(C) Strand-resolved RNA-seq coverage tracks at a region upstream to the *PCDHA* gene cluster of two arhinia patients (B1,Y1, and A1) and one control (D2). +, the plus strand. -, the minus strand.

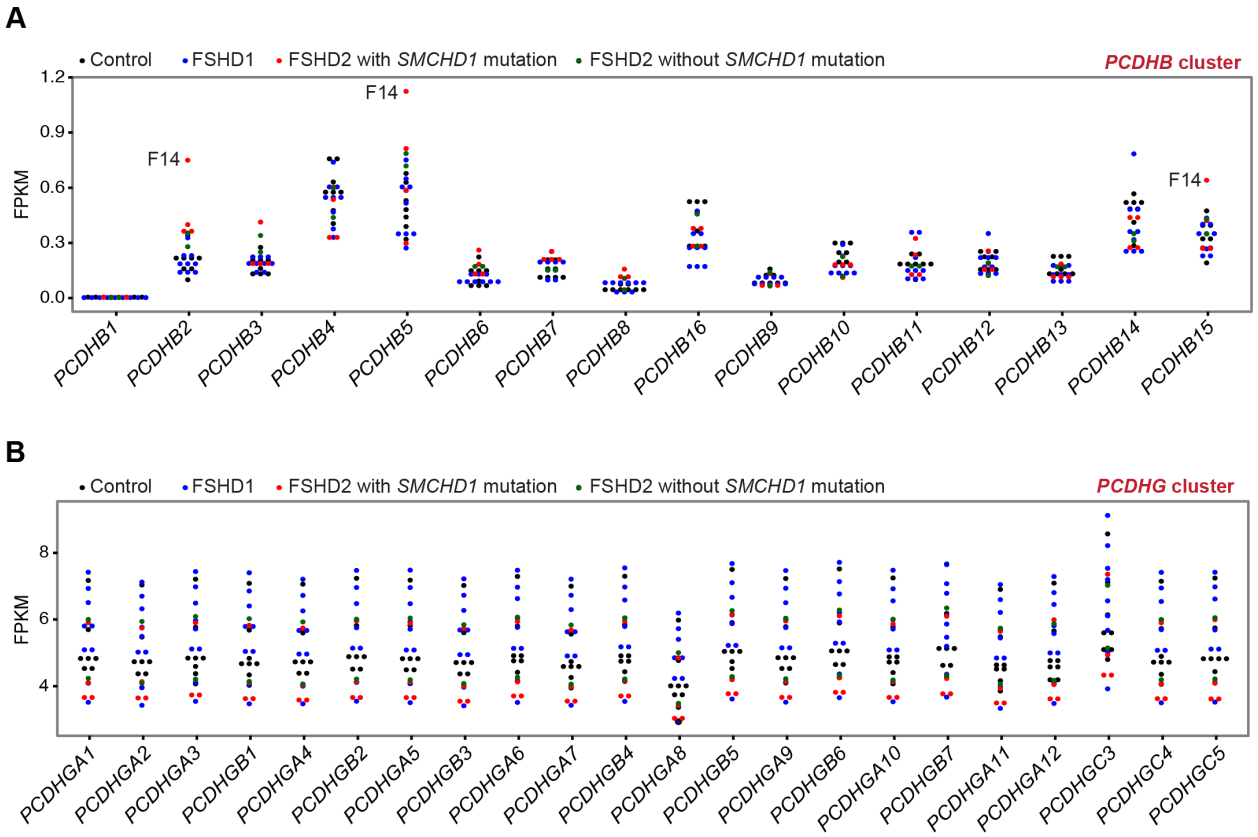

Figure S4. *PCDHB and PCDHG* expression in FSHD2 patients.

(A) Dot plots showing the FPKMs of the 16 *PCDHB* genes in muscle biopsies of 9 FSHD1 patients (blue), 3 FSHD2 patients carrying SMCHD1 mutations (red), 2 FSHD2 patients without SMCHD1 mutations (green), and 8 controls (black).

(B) Dot plots showing the FPKMs of the 22 *PCDHG* genes in the muscle biopsy cohort of FSHD.

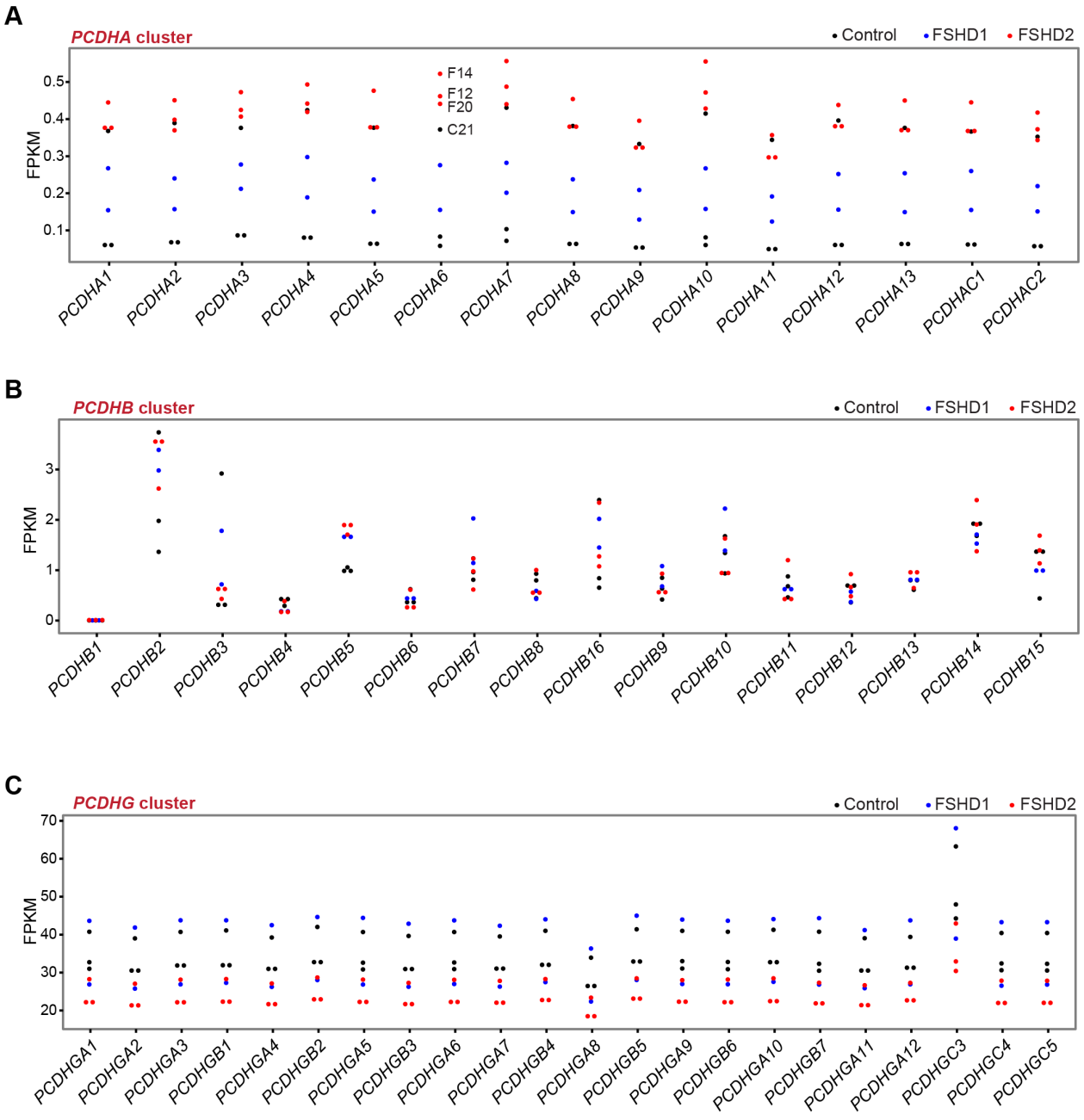

Figure S5. Slight upregulation of the *PCDHA* genes in the myotube culture of FSHD2 patient F14.

(A) Dot plots showing the FPKMs of the 14 *PCDHA* genes in *in vitro* cultured myotubes of 2 FSHD1 patients (blue), 3 FSHD2 patients carrying *SMCHD1* mutations (red), and 3 controls (black).

(B) Dot plots showing the FPKMs of the 16 *PCDHB* genes in the cohort of cultured FSHD myotubes.

(C) Dot plots showing the FPKMs of the 22 *PCDHG* genes in the cohort of cultured FSHD myotubes.

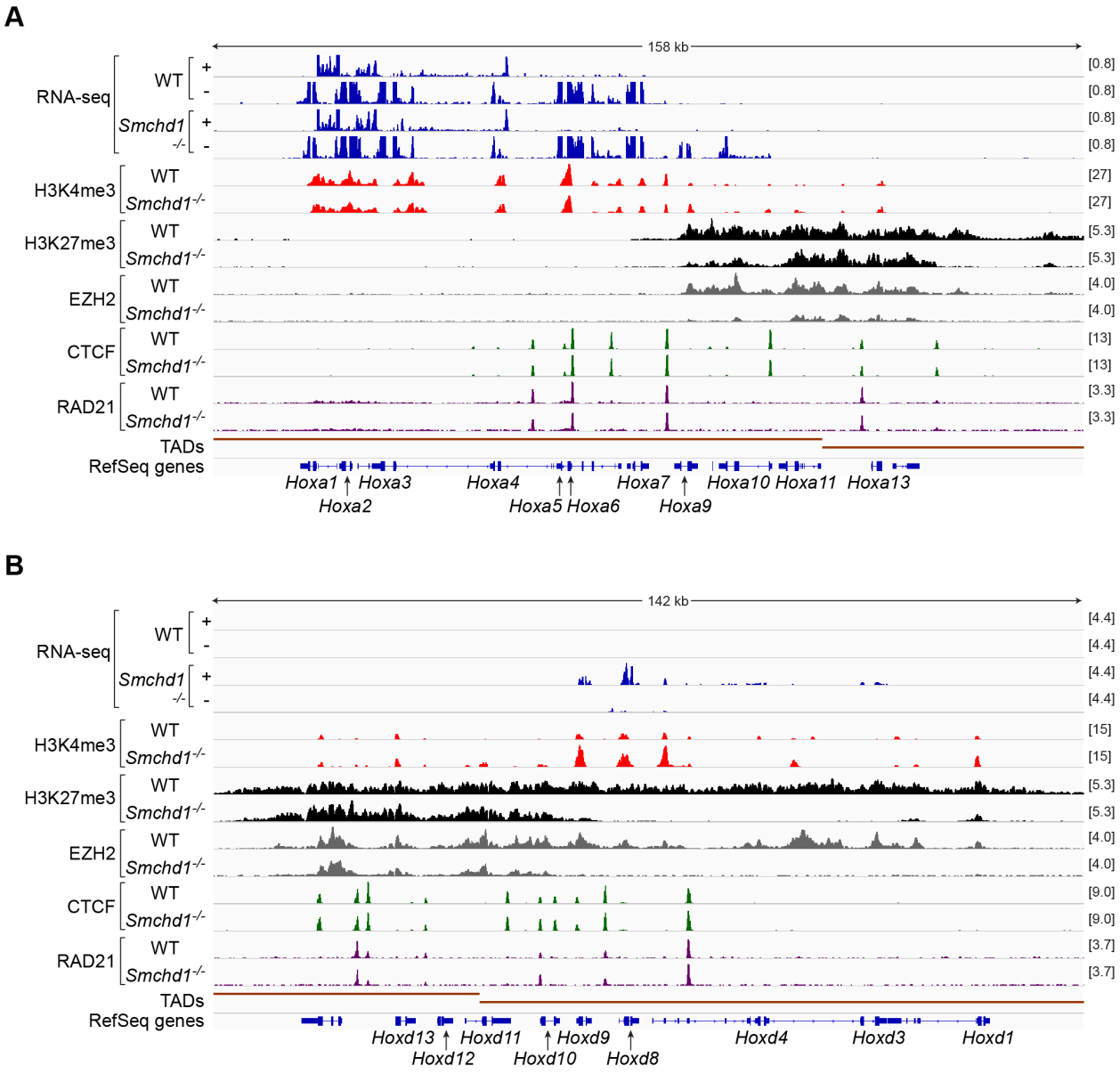

Figure S6. *Smchd1* ablation affects the expression and chromatin states of the *HoxA* and *HoxD* cluster in mice.

(A) RNA-seq, H3K4me3, H3K27me3, EZH2, CTCF, and RAD21 ChIP-seq (GSE99991) tracks at the *HoxA* cluster in WT and *Smchd1*$^{-/-}$ female mouse NPCs, with scales indicated in each track. Also shown are TADs defined in Dixon *et al*., 2012.

(B) RNA-seq, H3K4me3, H3K27me3, EZH2, CTCF, and RAD21 ChIP-seq (GSE99991) tracks at the *HoxD* cluster in WT and *Smchd1*$^{-/-}$ female mouse NPCs, with scales indicated in each track. Also shown are TADs defined in Dixon *et al*., 2012.

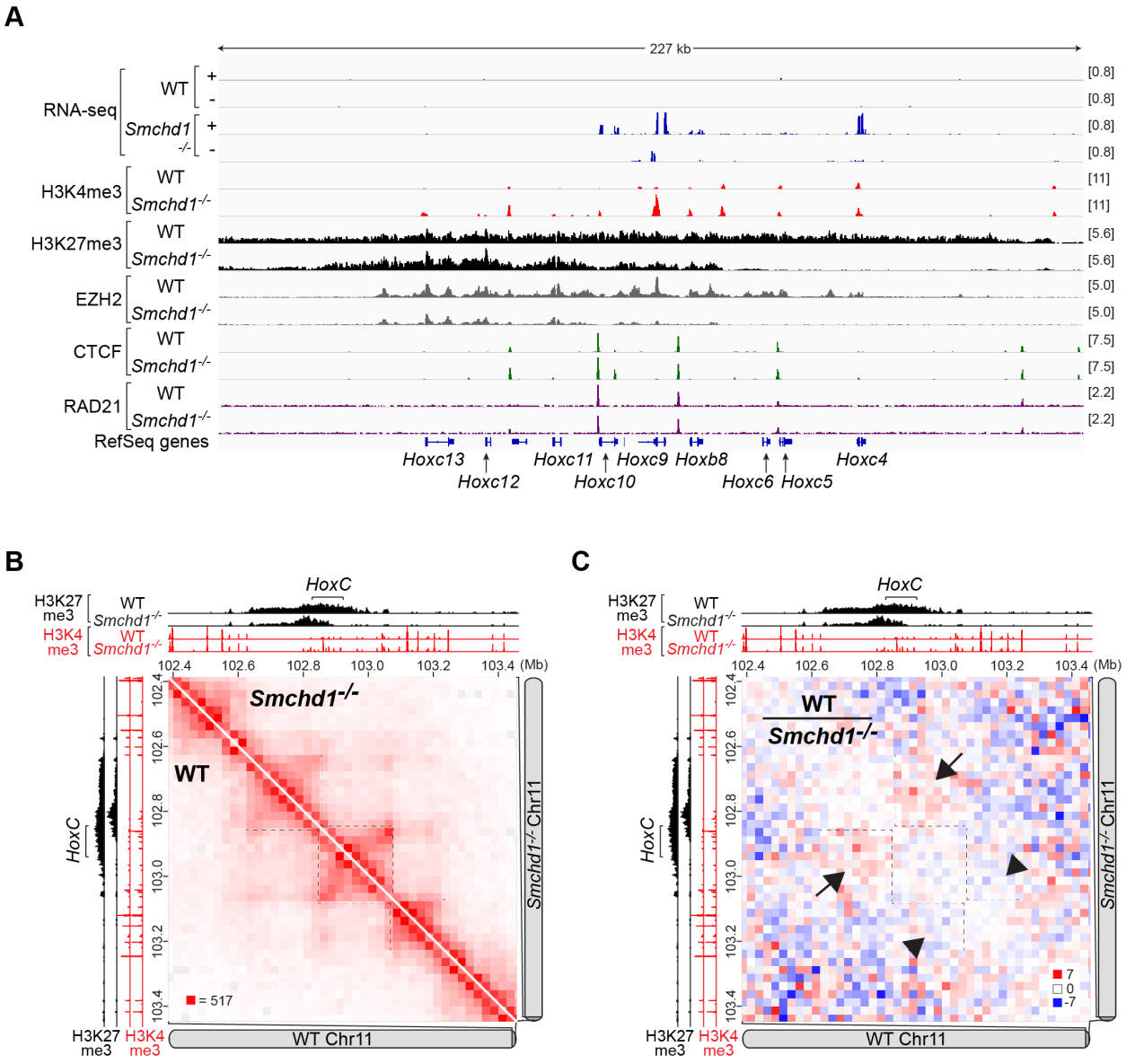

Figure S7. *Smchd1* ablation affects the expression, chromatin states, and 3D organization of *HoxC* cluster in mice.

(A) RNA-seq, H3K4me3, H3K27me3, Ezh2, CTCF, and RAD21 ChIP-seq (GSE99991) tracks at the *HoxC* cluster in WT and *Smchd1*$^{-/-}$ female mouse NPCs, with scales indicated in each track.

(B) Hi-C contact maps at 25-kb resolution at the *HoxC* cluster in WT (bottom) and *Smchd1*$^{-/-}$ (top) female mouse NPCs (GSE99991). Also shown are H3K4me3 and H3K27me3 ChIP-seq tracks in WT and *Smchd1*$^{-/-}$ female mouse NPCs.

(C) Differential Hi-C contact maps generated by dividing the WT with the *Smchd1*$^{-/-}$ contact map at 25-kb resolution at the *HoxC* cluster (GSE99991).